Blind Deconvolution of Graph Signals: Robustness to Graph Perturbations

Chang Ye, *Member, IEEE*, and Gonzalo Mateos, *Senior Member, IEEE*

***Abstract*—We study blind deconvolution of signals defined on the nodes of an undirected graph. Although observations are bilinear functions of both unknowns, namely the forward convolutional filter coefficients and the graph signal input, a filter invertibility requirement along with input sparsity allow for an efficient linear programming reformulation. Unlike prior art that relied on perfect knowledge of the graph eigenbasis, here we derive stable recovery conditions in the presence of small graph perturbations. We also contribute a provably convergent robust algorithm, which alternates between blind deconvolution of graph signals and eigenbasis denoising in the Stiefel manifold. Reproducible numerical tests showcase the algorithm's robustness under several graph eigenbasis perturbation models.**

***Index Terms*—Graph signal processing, robust blind deconvolution, graph perturbation, eigenbasis denoising, stable recovery.**

I. Introduction

CONSIDER an undirected network graph $\mathcal{G}(\mathcal{V},\mathcal{E})$, where $\mathcal{V}$ and $\mathcal{E}$ are the vertex and edge sets, respectively. Neural activities [1], [2], [3], vehicle trajectories [4], [5], [6], infectives due to an epidemic [7], [8], temperatures monitored by sensors [9], [10], or productivity of various economic sectors [11], [12], can all be represented as graph signals $\mathbf{x}\in\mathbb{R}^N$ on $\mathcal{V}$, where $|\mathcal{V}|=N$. Graph Signal Processing (GSP) deals with representations, filters, and algorithms that exploit the graph-induced relational structure of these signals [5], [13], [14]. Building on the graph shift operator (GSO) $\mathbf{S}\in\mathbb{R}^{N\times N}$ that encodes the graph topology, i.e., $S_{ij}=0$ if and only if $(i,j)\notin\mathcal{E}$, graph convolutional filters are polynomials $\mathbf{H}=\sum_{l=0}^{L-1}h_l\mathbf{S}^l$ that serve as local aggregation operators, with filter coefficients $\mathbf{h}=[h_0,\ldots,h_{L-1}]^\top\in\mathbb{R}^L$ [15], [16], [17].

In this context, here we revisit the blind deconvolution problem on graphs [8], [18]. Given P graph signals $\mathbf{Y}=[\mathbf{y}_1\ldots\mathbf{y}_P]\in\mathbb{R}^{N\times P}$ that we model as outputs of some polynomial graph filter $\mathbf{H}$ (where $\mathbf{S}$ is perfectly known, for now), the goal is to jointly identify the filter taps $\mathbf{h}$ and the latent signals $\mathbf{X}=[\mathbf{x}_1\ldots\mathbf{x}_P]$ driving the observations $\mathbf{y}_p=\mathbf{H}\mathbf{x}_p$, up to scaling. This bilinear inverse problem is ill-posed, so we assume $\mathbf{X}$ is sparse – say, as when few sources inject a signal that spreads on the graph [8]. In this letter, we study the robustness of existing and new blind deconvolution algorithms in the presence of graph perturbations.

Related work: Our starting point is a convex relaxation put forth in [18], feasible under a mild invertibility assumption on $\mathbf{H}$ (Section II) and inspired by the (graph-agnostic) blind deconvolution method in [19]. The algorithm in [18] outperforms its matrix-lifting precursor [8], and comes with exact recovery guarantees as well as noise stability bounds under the Bernoulli-Gaussian model for $\mathbf{X}$ [20]. However, [8], [18], [20] rely on perfect knowledge of the GSO (or its eigenbasis), and performance under pragmatic graph perturbations is yet to be explored. Resilience to imperfect topology information has received attention in other GSP contexts; noteworthy contributions include small perturbation analyses [21], [22], stability properties of graph neural networks (GNNs) [23], and topology denoising under signal and connectivity errors [24], [25]. Most germane to our work, [26] proposed a node-domain, non-convex blind deconvolution approach from multiple sparse signals on graphs with edge perturbations. Here, instead, we operate in the graph frequency domain and prove the method in [18] (which inspired [26] as well) is stable; see Section III.

Contributions: We derive a new stability result that ensures the filter estimation error remains manageable even when the eigenvectors of $\mathbf{S}$ (i.e., the graph Fourier basis) exhibit small perturbations. Modeling an imperfect graph eigenbasis is well motivated when e.g., the graph is unknown, but eigenvectors can still be estimated from stationary signals; see [27] and Remark 1. Our second main contribution is a robust blind deconvolution formulation and provably convergent optimization algorithm in the Stiefel manifold [28], to jointly "denoise" the given perturbed graph eigenbasis (Section IV). Numerical tests showcase the method's enhanced robustness relative to the blind deconvolution algorithms in [18], [26]. In the interest of reproducible research, we share the code used to generate all the figures in Section V. Concluding remarks are in Section VI. Due to page constraints, the proof of our main result is deferred to the accompanying Supplementary Material.

II. Preliminaries and Problem Statement

We begin by reviewing a convex relaxation approach to blind deconvolution on graphs, and state the exact recovery conditions derived in [20]. We then formulate and motivate the new problem arising when graph knowledge is imperfect.

Convex relaxation for invertible graph filters: Similar to [18], [20], [26], we henceforth assume the forward convolutional filter $\mathbf{H}$ is invertible. In such case, one can show that the inverse operator $\mathbf{G}:=\mathbf{H}^{-1}$ is also a graph filter on $\mathcal{G}$, which can be uniquely represented as a polynomial in $\mathbf{S}$ of degree at

Received 19 December 2024; revised 26 February 2025; accepted 8 March 2025. Date of publication 19 March 2025; date of current version 1 April 2025. This work was supported by the Center of Excellence in Data Science, an Empire State Development-Designated Center of Excellence. The associate editor coordinating the review of this article and approving it for publication was Prof. Tirza Routtenberg. *(Corresponding author: Gonzalo Mateos.)*

The authors are with the Department of ECE, University of Rochester, Rochester, NY 14627 USA (e-mail: gmateosb@ece.rochester.edu).

This article has supplementary downloadable material available at https://doi.org/10.1109/LSP.2025.3553064, provided by the authors.

Digital Object Identifier 10.1109/LSP.2025.3553064

most $N-1$ [15, Thm. 4]. To be more specific, let $\mathbf{g} \in \mathbb{R}^N$ be the vector of inverse-filter coefficients, i.e., $\mathbf{G} = \sum_{l=0}^{N-1} g_l \mathbf{S}^l$. Since $\mathbf{S}$ is symmetric, it is diagonalizable as $\mathbf{S} = \mathbf{V}\mathbf{\Lambda}\mathbf{V}^\top$, with $\mathbf{\Lambda} = \text{diag}(\lambda_1, \ldots, \lambda_N)$ collecting the eigenvalues and the eigenvectors $\mathbf{V}$ are akin to Fourier modes [5]. Accordingly, we equivalently rewrite the forward model $\mathbf{Y} = \mathbf{H}\mathbf{X}$ as $\mathbf{X} = \mathbf{G}\mathbf{Y} = \mathbf{V}\text{diag}(\tilde{\mathbf{g}})\mathbf{V}^\top\mathbf{Y}$, where $\tilde{\mathbf{g}} := \mathbf{\Psi}_N\mathbf{g} \in \mathbb{R}^N$ is the inverse filter's frequency response and $\mathbf{\Psi}_N \in \mathbb{R}^{N\times N}$ is Vandermonde with $\Psi_{ij} := \lambda_i^{j-1}$ [17].

Leveraging the invertibility of $\mathbf{H}$ and exploiting sparsity via an ℓ_1-norm criterion, [18] recasts the blind deconvolution task as a *convex and linear* inverse problem

$$\hat{\tilde{\mathbf{g}}} = \arg\min_{\tilde{\mathbf{g}}} \|\mathbf{V}\text{diag}(\tilde{\mathbf{g}})\mathbf{V}^\top\mathbf{Y}\|_{1,1}, \quad \text{s. to } \mathbf{1}_N^\top\tilde{\mathbf{g}} = N, \tag{1}$$

where $\|\mathbf{X}\|_{1,1} = \sum_{ij}|X_{ij}|$. The constraint in (1) excludes $\hat{\tilde{\mathbf{g}}} = \mathbf{0}_N$ and fixes the (arbitrary) scale of the solution; see [20]. Theoretical analysis of the convex estimator (1) is possible with the following tractable model for random sparse matrices.

Definition 1 (Bernoulli-Gaussian model): We say a random matrix $\mathbf{X} \in \mathbb{R}^{N\times P}$ adheres to the Bernoulli-Gaussian model with parameter $\theta \in (0,1)$, if $X_{ip} = \Omega_{ip}\gamma_{ip}/\sqrt{\theta}$, where $\Omega_{ip} \sim$ Bernoulli(θ) and $\gamma_{ip} \sim$ Normal$(0,1)$ are i.i.d. for all i, p.

Let $\mathbf{P}_1^\perp := \mathbf{I}_N - \frac{\mathbf{1}_N\mathbf{1}_N^\top}{N}$ be the projection onto span$^\perp(\mathbf{1}_N)$ and define matrix $\tilde{\mathbf{U}} := (\mathbf{V}\circ\mathbf{V})\mathbf{P}_1^\perp \in \mathbb{R}^{N\times N}$, where $\circ$ denotes the Hadamard product. One can show the spectral radius $\sigma_{\max}(\tilde{\mathbf{U}}) \le 1$. The ensuing theorem offers a sufficient condition under which (1) succeeds with high probability.

Theorem 1 (Exact recovery [20]): Consider graph signal observations $\mathbf{Y} = \mathbf{V}\text{diag}(\tilde{\mathbf{h}}_0)\mathbf{V}^\top\mathbf{X}_0 \in \mathbb{R}^{N\times P}$, where $\mathbf{X}_0$ adheres to the Bernoulli-Gaussian model with $\theta \in (0, 0.324]$ and $\tilde{\mathbf{h}}_0 \circ \tilde{\mathbf{g}}_0 = \mathbf{1}_N$. Let $P \ge C'\sigma_m^{-2}\log\frac{4}{\delta}$, where $\sigma_m = \min(\sigma_1, \sigma_2, \sigma_3, \sigma_4)$ and $\sigma_1 \in \left(0, \frac{\sqrt{\pi}\theta^{3/2}}{2}\right]$, $\sigma_2 \in \left(0, \frac{\sqrt{\pi}\theta}{2}\right]$, $\sigma_3 > 0$, $\sigma_4 \in (0,1)$, $\delta \in (0,1)$ are parameters, while C' is a constant that does not depend on P, σ_m, or δ. Then $\hat{\tilde{\mathbf{g}}} = \tilde{\mathbf{g}}_0$ is the unique solution to (1) with probability at least $1-\delta$, if

$$\left\|\mathbf{P}_1^\perp\tilde{\mathbf{g}}_0\right\|_2 \le a_0, \tag{2}$$

where $a_0 := \frac{\sqrt{1-\sigma_{\max}^2(\tilde{\mathbf{U}})}[(1-\sigma_1)-2\theta(1+\sigma_2)](1-\sigma_4)}{(1+\sigma_3)\sqrt{\theta}}$.

From (2), one can interpret $\|\mathbf{P}_1^\perp\tilde{\mathbf{g}}_0\|_2$ as a measure of the filter's (and the problem's) ill-conditioning. Moreover, increasing θ within its feasible range will decrease a_0, thus challenging recovery. Please refer to [20] for an expanded discussion.

Problem statement: Going beyond prior algorithmic [18], [26] and theoretical studies [8], [20] of blind deconvolution on graphs, in this letter we investigate the robustness of (1) when the knowledge of $\mathcal{G}$ is imperfect. There have been several graph perturbation models considered in the GSP literature [21], [22], [23], [24], [25], [26], but given the spectral domain approach (1) we directly focus on perturbations $\mathbf{\Delta} = \mathbf{V} - \mathbf{V}_p$ to the graph's eigenbasis $\mathbf{V}$. Given observations $\mathbf{Y} = \mathbf{V}\text{diag}(\tilde{\mathbf{h}})\mathbf{V}^\top\mathbf{X}$ and *perturbed* GSO eigenvectors $\mathbf{V}_p$ ($\mathbf{S}$ is no longer perfectly known), we ask what is the performance of [cf. (1)]

$$\hat{\tilde{\mathbf{g}}}_p = \arg\min_{\tilde{\mathbf{g}}} \|\mathbf{V}_p\text{diag}(\tilde{\mathbf{g}})\mathbf{V}_p^\top\mathbf{Y}\|_{1,1}, \quad \text{s. to } \mathbf{1}_N^\top\tilde{\mathbf{g}} = N. \tag{3}$$

Remark 1 (Motivating graph eigenbasis perturbations): Even when the graph topology $\mathbf{S}$ is completely unknown, under the Bernoulli-Gaussian model (Definition 1) one can still (imperfectly) estimate the graph eigenvectors from the observations $\mathbf{Y} = \mathbf{H}\mathbf{X}$. Indeed, since $\mathbf{C}_x := \mathbb{E}[\mathbf{x}_p\mathbf{x}_p^\top] = \mathbf{I}_N$, the ensemble covariance matrix of the observations is

$$\mathbf{C}_y := \mathbb{E}\left[\mathbf{y}_p\mathbf{y}_p^\top\right] = \mathbf{H}\mathbb{E}\left[\mathbf{x}_p\mathbf{x}_p^\top\right]\mathbf{H}^\top = \mathbf{V}\text{diag}^2(\tilde{\mathbf{h}})\mathbf{V}^\top.$$

The conclusion is that the GSO eigenvectors coincide with those of $\mathbf{C}_y$, and one can form an estimate $\mathbf{V}_p$ by diagonalizing the sample covariance matrix $\hat{\mathbf{C}}_y = \frac{\mathbf{Y}\mathbf{Y}^\top}{P-1}$; see also [27].

III. Stable Recovery Under Graph Perturbations

Our main stable recovery result asserts that the estimation error on the inverse filter's frequency response can be kept at a manageable level, even when the given GSO eigenbasis is subject to small errors $\mathbf{\Delta} = \mathbf{V} - \mathbf{V}_p$. Recalling the statement and conditions of Theorem 1, let $\mathcal{S} := \text{supp}(\mathbf{X}_0) = \text{supp}(\mathbf{\Omega})$. Defining $\mathbf{E} := (\mathbf{V}-\mathbf{\Delta})[\mathbf{\Delta}^\top - \text{diag}(\tilde{\mathbf{g}}_0)\mathbf{\Delta}^\top\mathbf{H}_0]\mathbf{X}_0 \in \mathbb{R}^{N\times P}$, let $\mathbf{E}^{(\mathcal{S}^C)} := \mathbf{E}\circ(\mathbf{1}_{N\times N} - \mathbf{\Omega})$ be the restriction to the entries in the complement $\mathcal{S}^C$ of the support of $\mathbf{X}_0$. We can thus establish the following error bound for the solution of (3).

Theorem 2 (Stable recovery to graph perturbations): Consider the same setting and conditions in Theorem 1, including (2) for $a_0 \ge 0$ that does not depend on $\mathbf{\Delta}$. Then the estimation error associated to the solution $\hat{\tilde{\mathbf{g}}}_p$ of (3) is bounded by

$$\left\|\hat{\tilde{\mathbf{g}}}_p - \tilde{\mathbf{g}}_0\right\|_2 \le \frac{2\sigma_{\max}\left(\text{diag}(\tilde{\mathbf{g}}_0) - \frac{\tilde{\mathbf{g}}_0\tilde{\mathbf{g}}_0^\top}{N}\right)\|\mathbf{E}^{(\mathcal{S}^C)}\|_{1,1}}{PQ - a_0\|\mathbf{E}^{(\mathcal{S}^C)}\|_{1,1} - \|[\mathbf{E}^{(\mathcal{S}^C)}]^\top\mathbf{V}\odot\mathbf{V}\|_{1\to 2}}, \tag{4}$$

where $Q := C_1\sqrt{\theta}(\sqrt{a_0^2 - (1-\sigma)^2\|\mathbf{P}_1^\perp\tilde{\mathbf{g}}_0\|_2^2} - \sigma\|\mathbf{P}_1^\perp\tilde{\mathbf{g}}_0\|_2)$ for some $\sigma \in [0,1]$ and $C_1 > 0$. The operator norm $\|\cdot\|_{1\to 2}$ denotes the maximum ℓ_2-norm for the columns of its matrix argument, and $\odot$ stands for the Kathri-Rao product.

Proof: Included in the Supplementary Material. ■

Notice first that $Q \ge 0$, because $\|\mathbf{P}_1^\perp\tilde{\mathbf{g}}_0\|_2 \le a_0$ as per (2). Importantly, the denominator in the right-hand side of (4) should be non-negative to obtain a feasible upper bound. This effectively imposes a constraint on the magnitude of the error component $\mathbf{E}^{(\mathcal{S}^C)}$, which should satisfy

$$\|\mathbf{E}^{(\mathcal{S}^C)}\|_F \le PQ/M_1, \tag{5}$$

where $M_1 := a_0\|\bar{\mathbf{E}}^{(\mathcal{S}^C)}\|_{1,1} + \|[\bar{\mathbf{E}}^{(\mathcal{S}^C)}]^\top\mathbf{V}\odot\mathbf{V}\|_{1\to 2}$ and $\bar{\mathbf{E}}^{(\mathcal{S}^C)} := \mathbf{E}^{(\mathcal{S}^C)}/\|\mathbf{E}^{(\mathcal{S}^C)}\|_F$. A sufficient condition for (5) to hold is that $\|\mathbf{E}\|_F \le PQ/M_1$, since $\|\mathbf{E}^{(\mathcal{S}^C)}\|_F \le \|\mathbf{E}\|_F$. Because $\|\mathbf{E}\|_F$ is proportional to the magnitude of $\mathbf{\Delta}$, namely

$$\|\mathbf{E}\|_F = \|[\mathbf{\Delta}^\top - \text{diag}(\tilde{\mathbf{g}}_0)\mathbf{\Delta}^\top\mathbf{H}_0]\mathbf{X}_0\|_F = M_2\|\mathbf{\Delta}\|_F,$$

where $M_2 := \|[\bar{\mathbf{\Delta}}^\top - \text{diag}(\tilde{\mathbf{g}}_0)\bar{\mathbf{\Delta}}^\top\mathbf{H}_0]\mathbf{X}_0\|_F$ and $\bar{\mathbf{\Delta}} := \mathbf{\Delta}/\|\mathbf{\Delta}\|_F$, then we can upper bound $\|\mathbf{\Delta}\|_F$ as

$$\|\mathbf{\Delta}\|_F \le PQ/(M_1M_2). \tag{6}$$

The right-hand side of (6) provides an upper bound to the magnitude of the eigenbasis perturbation that is tolerable. Again, in the favorable setting where $\|\mathbf{P}_1^\perp\tilde{\mathbf{g}}_0\|_2$ is small, e.g., if $\tilde{\mathbf{g}}_0$ is closer to the all-ones vector $\mathbf{1}_N$, we will have a larger upper bound in (6) because Q increases and M_2 decreases.

IV. Robust Blind Deconvolution Algorithm

Theorem 2 shows the convex relaxation (1) is robust to small errors $\mathbf{\Delta}$ in the GSO eigenbasis, complementing the noise stability results in [20]. Here we develop a new robust blind deconvolution formulation and associated algorithm to jointly

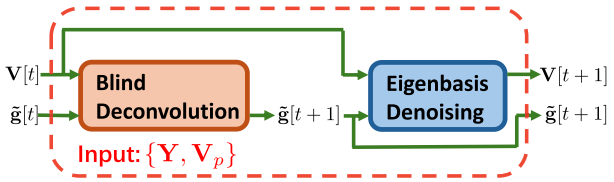

Fig. 1. Schematic diagram of an iteration of the robust blind deconvolution of graph signals (RBDoGS) algorithm.

estimate $\tilde{\mathbf{g}}$ and denoise $\mathbf{V}_p$. In Section V we empirically show it outperforms (3), especially for larger perturbations.

Our idea is to adopt the Huber loss [29] (with small $\epsilon \geq 0$)

$$h_\epsilon(x) := \begin{cases} \frac{x^2}{2\epsilon}, & |x| < \epsilon \\ |x| - \frac{\epsilon}{2}, & |x| \geq \epsilon \end{cases} \tag{7}$$

in order to construct a smooth surrogate $f(\tilde{\mathbf{g}}, \mathbf{V}) := \sum_{i,j} h_\epsilon(\mathbf{e}_i^\top \mathbf{V} \text{diag}(\tilde{\mathbf{g}}) \mathbf{V}^\top \mathbf{y}_j)$ to the cost function in (1), where $\mathbf{e}_i$ is the i-th coordinate vector. Note that $f(\tilde{\mathbf{g}}, \mathbf{V})$ is differentiable with a Lipschitz gradient and $f(\tilde{\mathbf{g}}, \mathbf{V}) \leq \|\mathbf{V}\text{diag}(\tilde{\mathbf{g}})\mathbf{V}^\top \mathbf{Y}\|_{1,1} \leq f(\tilde{\mathbf{g}}, \mathbf{V}) + \frac{\epsilon}{2}$. Accordingly, we propose to solve the following smooth, manifold-constrained problem

$$\min_{\tilde{\mathbf{g}}, \mathbf{V} \in \mathcal{M}_{St}} \underbrace{\left\{ f(\tilde{\mathbf{g}}, \mathbf{V}) + \frac{\rho}{2} \|\mathbf{V} - \mathbf{V}_p\|_F^2 \right\}}_{:= F(\tilde{\mathbf{g}}, \mathbf{V})}, \quad \text{s. to } \mathbf{1}_N^\top \tilde{\mathbf{g}} = N, \tag{8}$$

where $\mathcal{M}_{St} = \{\mathbf{V} \in \mathbb{R}^{N \times N} \mid \mathbf{V}^\top \mathbf{V} = \mathbf{I}_N\}$ is the Stiefel manifold of orthogonal matrices. Importantly, we *jointly* optimize over the inverse filter frequency response and the denoised graph eigenvectors, using a criterion $F(\tilde{\mathbf{g}}, \mathbf{V})$ that combines data consistency and encourages similarity to the given $\mathbf{V}_p$.

Solving (8) is challenging since the problem is non-convex. Yet its structure lends itself naturally to an iterative block-coordinate descent approach in the Stiefel manifold [28]. At iteration $t = 0, 1, 2, \ldots$ we blend: (i) block exact minimization of (8) w.r.t. $\tilde{\mathbf{g}}$ for fixed $\mathbf{V}[t]$ to obtain $\tilde{\mathbf{g}}[t+1]$; and (ii) then perform one step of block Riemannian gradient descent (BRGD) w.r.t. $\mathbf{V}$ to update $\mathbf{V}[t+1]$. The update steps (i)-(ii) are detailed below and also schematically illustrated in Fig. 1.

Blind deconvolution: At step (i) of iteration t, we compute a minimizer $\tilde{\mathbf{g}}[t+1]$ of $F(\tilde{\mathbf{g}}, \mathbf{V}[t])$ by solving the smoothed convex blind deconvolution subproblem,

$$\tilde{\mathbf{g}}[t+1] = \text{argmin}_{\tilde{\mathbf{g}}} f(\tilde{\mathbf{g}}, \mathbf{V}[t]), \quad \text{s. to } \mathbf{1}_N^\top \tilde{\mathbf{g}} = N, \tag{9}$$

where $\mathbf{V}[t]$ is the eigenbasis estimate from iteration $t-1$. In practice, we can also obtain $\tilde{\mathbf{g}}[t+1]$ by solving (3) with $\mathbf{V}_p = \mathbf{V}[t]$, since (3) and (9) are equivalent when $\epsilon \to 0$.

Eigenbasis denoising: At step (ii), computational considerations motivate applying a single iteration of BRGD to update

$$\mathbf{V}[t+1] = \text{Retr}_{\mathbf{V}[t]}(-\beta_t \tilde{\nabla}_{\mathbf{V}} F(\tilde{\mathbf{g}}[t+1], \mathbf{V}[t])), \tag{10}$$

where $\text{Retr}_{\mathbf{V}[t]}(\cdot)$ is the retraction mapping at $\mathbf{V}[t]$, $\tilde{\nabla}_{\mathbf{V}} F(\cdot, \cdot)$ is the Riemannian gradient w.r.t. $\mathbf{V}$, and β_t is a step size. Update (10) can be computed via the Cayley transform $\mathbf{V}[t+1] = \mathcal{C}(\mathbf{M}[t])\mathbf{V}[t]$; see e.g., [30, Example 3.6.2], where

$$\mathbf{G}[t] = \nabla_{\mathbf{V}} F(\tilde{\mathbf{g}}[t+1], \mathbf{V}[t]),$$

$$\mathbf{M}[t] = \mathbf{G}[t]\mathbf{V}^\top[t] - \mathbf{V}[t]\mathbf{G}^\top[t],$$

$$\mathcal{C}(\mathbf{M}[t]) = \left(\mathbf{I}_N + \frac{\beta_t}{2}\mathbf{M}[t]\right)^{-1} \left(\mathbf{I}_N - \frac{\beta_t}{2}\mathbf{M}[t]\right). \tag{11}$$

Algorithm 1: Robust Blind Deconvolution of Graph Signals.

1: **Input:** $\mathbf{Y}$, $\mathbf{V}_p$, $\delta > 0$ and $\epsilon > 0$.
2: **Initialize** $t = 0$, $\mathbf{V}[0] = \mathbf{V}_p$, $\tilde{\mathbf{g}}[0] = \mathbf{1}_N$.
3: **repeat**
4: Update $\tilde{\mathbf{g}}[t]$ by solving (9).
5: Update $\mathbf{V}[t]$ via BRGD in (10); e.g. using (11).
6: $t \leftarrow t + 1$.
7: **until** $\|\tilde{\mathbf{g}}[t] - \tilde{\mathbf{g}}[t-1]\|_2 \leq \delta$ and $\|\mathbf{V}[t] - \mathbf{V}[t-1]\|_2 \leq \delta$.
8: **return** $\hat{\tilde{\mathbf{g}}} := \tilde{\mathbf{g}}^{(t)}$ and $\hat{\mathbf{X}} := \mathbf{V}[t]\text{diag}(\tilde{\mathbf{g}}[t])\mathbf{V}[t]^\top \mathbf{Y}$.

The procedure in (11) connects the Euclidean gradient $\mathbf{G}[t]$ of $F(\cdot, \cdot)$ and its BRGD direction that ensures $\mathbf{V}[t+1] \in \mathcal{M}_{St}$. We determine the step size β_t via line search [31]. The pseudo-code of the novel algorithm for robust blind deconvolution of graph signals (RBDoGS) is tabulated under Algorithm 1.

The computational complexity of RBDoGS is $\mathcal{O}(N^3)$ per iteration. Because (9) has a unique minimizer and $F(\cdot, \cdot)$ is block-i Lipschitz smooth [28, Definition 4] w.r.t. $\mathbf{V}$, then convergence of Algorithm 1 follows from [28, Thm. 4].

V. Numerical Experiments

For all the experiments in this section we consider Erdös-Renyi random graphs with $N = 20$ nodes and edge formation probability $p_\mathcal{E} = 0.4$. We select the degree-normalized adjacency matrix as the GSO, i.e. $\mathbf{S} = \mathbf{D}^{-1/2}\mathbf{A}\mathbf{D}^{-1/2}$, where $\mathbf{D} = \text{diag}(\mathbf{A}\mathbf{1}_N)$. Implementation details are in the public code[1], which can be run to generate all plots in Figs. 2 and 3.

Test case 1. Controllable $\|\mathbf{P}_1^\perp \tilde{\mathbf{g}}_0\|_2$ and $\|\mathbf{\Delta}\|_F$: We draw inputs $\mathbf{X}_0 \in \mathbb{R}^{N \times P}$ from the Bernoulli-Gaussian model, with $P = 60$ and $\theta = 0.15$. The graph filter $\mathbf{H}_0 = \mathbf{V}\text{diag}(\tilde{\mathbf{h}}_0)\mathbf{V}^\top$ is generated such that $\tilde{\mathbf{g}}_0 = \mathbf{1}_N + (\alpha \mathbf{P}_1^\perp \mathbf{b})/\|\mathbf{P}_1^\perp \mathbf{b}\|_2$, where $\mathbf{b} \sim \text{Normal}(\mathbf{0}_N, \mathbf{I}_N)$. This way we can control $\|\mathbf{P}_1^\perp \tilde{\mathbf{g}}_0\|_2 = \alpha$, and larger α leads to a harder blind deconvolution problem [cf. (2)]. The observations are generated as $\mathbf{Y} = \mathbf{H}_0 \mathbf{X}_0$.

In order to simulate graph perturbations with controllable $\|\mathbf{\Delta}\|_F$, we apply the parameterized Cayley transformation $\mathcal{C}(\mathbf{W}, \xi) := (\mathbf{I}_N + \xi \mathbf{W})^{-1}(\mathbf{I}_N - \xi \mathbf{W})$ to $\mathbf{V}$, with parameter $\xi \in [0, \infty)$ and a skew-symmetric matrix $\mathbf{W}$ with unit Frobenius norm. We generate $\mathbf{V}_p = \mathcal{C}(\mathbf{W}, \xi)\mathbf{V}$. The eigenvalues of $\mathbf{W}$ are all imaginary, i.e., $\{i\mu_k\}_{k=1}^N$. Then one can derive

$$\|\mathbf{\Delta}\|_F^2 = \|[\mathbf{I}_N - \mathcal{C}(\mathbf{W}, \xi)]\mathbf{V}\|_F^2 = \sum_{k=1}^N \frac{4\mu_k^2}{\frac{1}{\xi^2} + \mu_k^2}, \tag{12}$$

so $\|\mathbf{\Delta}\|_F^2$ varies from 0 to $4N$ when ξ varies from 0 to ∞. We run Algorithm 1 with inputs $\{\mathbf{Y}, \mathbf{V}_p\}$, for different values of α and ξ. To assess the robustness of RBDoGS, we use the convex blind deconvolution on graphs (BDoG) estimator (3) as baseline [18]. As figures of merit we adopt the root mean square error (RMSE) $\text{RE}_g := \|\hat{\tilde{\mathbf{g}}} - \tilde{\mathbf{g}}_0\|_2 / \|\tilde{\mathbf{g}}_0\|_2$ and the support recovery accuracy $\text{ACC}_X := \frac{|\text{supp}_\tau(\hat{\mathbf{X}}) \cap \text{supp}_\tau(\mathbf{X}_0)|}{|\text{supp}_\tau(\mathbf{X}_0)|}$, where $\text{supp}_\tau(\cdot)$ is the support function with threshold $\tau = 0.1$. The results are shown in Fig. 2, where (a) and (c) are $1 - \text{RE}_g$ for RBDoGS and (3), respectively. Apparently, for the convex approach (3) in [18], [20], the recovery performance $1 - \text{RE}_g$ is decent for small ξ [cf. Theorem 2],

[1]The code is available from: https://hajim.rochester.edu/ece/sites/gmateos/code/RBDoGS.zip.

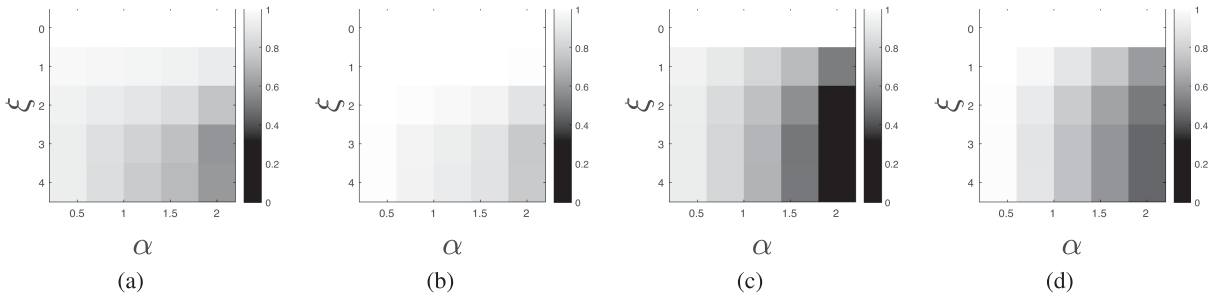

Fig. 2. Improved recovery performance of the RBDoGS algorithm on Erdös-Renyi random graphs with $N = 20$, $P = 60$, $p_{\mathcal{E}} = 0.4$, as a function of $\alpha = \|\mathbf{P}_1^{\perp}\tilde{\mathbf{g}}_0\|_2$ and $\xi = \|\mathbf{\Delta}\|_F$. (a) and (b) show $1 - \text{RE}_g$ and ACC_X for Algorithm 1 (the whiter the better). (c) and (d) show $1 - \text{RE}_g$ and ACC_X for the BDoG baseline that solves (3) with an imperfect $\mathbf{V}_p$ [18]. Results depict averages over 100 independent realizations.

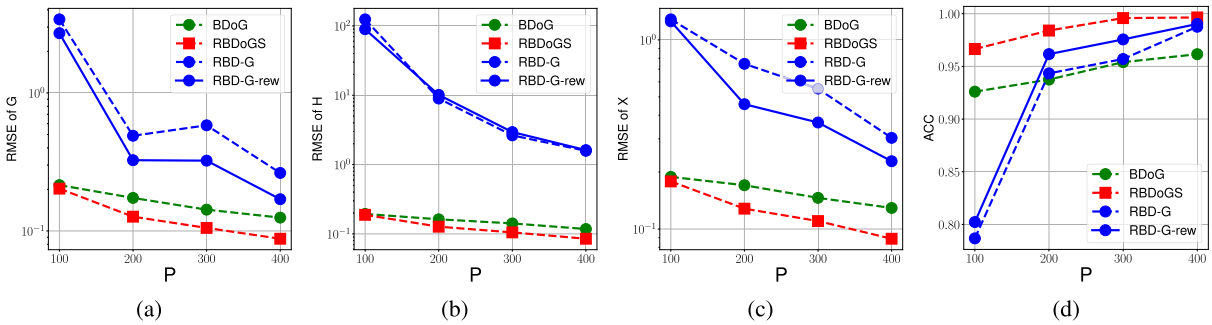

Fig. 3. Improved recovery performance of the RBDoGS algorithm on Erdös-Renyi random graphs with $N = 20$, $p_{\mathcal{E}} = 0.4$, as a function of the sample size P. (a) - (c) show the RMSE of $\mathbf{G}$, $\mathbf{H}$, $\mathbf{X}$, respectively; and (d) shows ACC_X for four competing approaches, including the BDoG baseline that solves (3) with an imperfect $\mathbf{V}_p$ [18], the proposed RBDoGS, the RBD-G algorithm and its variant RBD-G-rew in [26]. Median results over 20 independent realizations.

but it worsens rapidly as ξ increases. Especially for a larger α, the eigenbasis error proxy ξ has greater impact on the decrease of the recovery performance of (3). This is consistent with Theorem 2, since a larger α reduces Q, leading to a lower bound (6) for $\|\mathbf{\Delta}\|_F$ (and also ξ). RBDoG attains markedly better RMSE. For small ξ, the recovery error of $\hat{\tilde{\mathbf{g}}}$ is still small – even for larger α. Small perturbation of $\mathbf{V}$ can be almost perfectly corrected by the RBDoGS algorithm. By comparing (a) and (c), one can conclude that Algorithm 1 significantly improves the recovery performance when ξ is larger. From Fig. 2(b) and (d), ACC_X trends are consistent with our discussion for the RMSE.

Test case 2. Covariance matrix eigenvector: To assess recovery performance in the scenario of Remark 1, we generate Bernoulli-Gaussian distributed sources $\mathbf{X}_0$ with $\theta = 0.15$, for different sample sizes P. Instead of constructing an inverse filter $\mathbf{G}_0$, we directly generate the filter $\mathbf{H}_0 = \sum_{l=0}^{L-1} h_l \mathbf{S}^l$ with coefficients $\mathbf{h} = \mathbf{e}_1 + \mathbf{h}'$, where $\mathbf{e}_1 = [1, 0, \ldots, 0]^\top \in \mathbb{R}^L$ for $L = 5$ and $\mathbf{h}' \sim \text{Normal}(\mathbf{0}_L, \mathbf{I}_L)$ (then normalized $\|\mathbf{h}'\|_2 = 1$). Once more, the observations are generated as $\mathbf{Y} = \mathbf{H}_0\mathbf{X}_0$.

For comparison, we also implement the BDoG approach in [18] and two recent blind deconvolution methods in [26] that are robust to edge perturbations, i.e., RBD-G and RBD-G-rew. Results are depicted in Fig. 3. Apparently, RBD-G and RBD-G-rew suffer from the fact that the edgewise perturbation model is not ideal to capture the difference between $\hat{\mathbf{C}}_y$ and the true GSO. Hence the RMSE in (a)–(c), i.e., $\text{RE}_H = \|\hat{\mathbf{H}}_0 - \mathbf{H}_0)\|_F / \|\mathbf{H}_0\|_F$, likewise RE_G and RE_X, all attain fairly high values (> 0.1). However, for ACC_X, both algorithms still achieve acceptable performance above 0.8. For BDoG (no eigenvector denoising), the RMSE of $\mathbf{G}, \mathbf{H}$ and $\mathbf{X}$ is moderate and around 0.1, consistent with Theorem 2. RBDoGS outperforms all of the other three baselines and consistently attains the lowest RMSE. Moreover, Fig. 3(d) shows that it almost perfectly identifies the support of $\mathbf{X}_0$. While (8) is non-convex, Algorithm 1 markedly reduces error with proper initialization $\mathbf{V}_p$ extracted from $\hat{\mathbf{C}}_y$.

VI. Concluding Remarks

We studied robustness of blind deconvolution on networks, when required spectral graph information is imperfect. For the BDoG method in [18], [20], we established a stable recovery result by deriving an error bound that holds when the GSO eigenbasis perturbation is small. We also contributed a new robust formulation and associated RBDoGS algorithm to jointly recover the inverse filter and sparse latents, aided by graph eigenbasis denoising. Numerical experiments show that RBDoGS compares favorably w.r.t. state-of-the-art approaches, especially for larger perturbations. Ongoing and future work includes generalizations to directed graphs [32], scalable online algorithms for streaming data, and GSP-aware supervised learning models leveraging the algorithm unrolling principle [33].

References

[1] W. Huang, L. Goldsberry, N. F. Wymbs, S. T. Grafton, D. S. Bassett, and A. Ribeiro, "Graph frequency analysis of brain signals," *IEEE J. Sel. Topics Signal Process.*, vol. 10, no. 7, pp. 1189–1203, Oct. 2016.

[2] C. Hu, X. Hua, J. Ying, P. M. Thompson, G. E. Fakhri, and Q. Li, "Localizing sources of brain disease progression with network diffusion model," *IEEE J. Sel. Topics Signal Process.*, vol. 10, no. 7, pp. 1214–1225, Oct. 2016.

[3] S. S. Saboksayr, G. Mateos, and M. Cetin, "Online discriminative graph learning from multi-class smooth signals," *Signal Process.*, vol. 186, 2021, Art. no. 108101.
[4] J. A. Deri and J. M. F. Moura, "New york city taxi analysis with graph signal processing," in *Proc. IEEE Glob. Conf. Signal Inf. Process*., Dec. 2016, pp. 1275–1279.
[5] A. Ortega, P. Frossard, J. Kovačević, J. M. F. Moura, and P. Vandergheynst, "Graph signal processing: Overview, challenges, and applications," *Proc. IEEE*, vol. 106, no. 5, pp. 808–828, May 2018.
[6] R. Shafipour, S. Segarra, A. G. Marques, and G. Mateos, "Identifying the topology of undirected networks from diffused non-stationary graph signals," *IEEE Open J. Signal Process.*, vol. 2, pp. 171–189, 2021.
[7] Y. Li and G. Mateos, "Graph frequency analysis of COVID-19 incidence to identify county-level contagion patterns in the United States," in *Proc. Int. Conf. Acoust., Speech, Signal Process*., 2021, pp. 3230–3234.
[8] S. Segarra, G. Mateos, A. G. Marques, and A. Ribeiro, "Blind identification of graph filters," *IEEE Trans. Signal Process.*, vol. 65, no. 5, pp. 1146–1159, Mar. 2017.
[9] X. Dong, D. Thanou, P. Frossard, and P. Vandergheynst, "Learning Laplacian matrix in smooth graph signal representations," *IEEE Trans. Signal Process.*, vol. 64, no. 23, pp. 6160–6173, Dec. 2016.
[10] Z. Xiao, H. Fang, S. Tomasin, G. Mateos, and X. Wang, "Joint sampling and reconstruction of time-varying signals over directed graphs," *IEEE Trans. Signal Process.*, vol. 71, pp. 2204–2219, 2023.
[11] A. G. Marques, S. Segarra, G. Leus, and A. Ribeiro, "Sampling of graph signals with successive local aggregations," *IEEE Trans. Signal Process.*, vol. 64, no. 7, pp. 1832–1843, Apr. 2016.
[12] A. Hashemi, R. Shafipour, H. Vikalo, and G. Mateos, "Towards accelerated greedy sampling and reconstruction of bandlimited graph signals," *Signal Process.*, vol. 195, 2022, Art. no. 108505.
[13] L. Stankovic, D. P. Mandic, M. Dakovic, I. Kisil, E. Sejdic, and A. G. Constantinides, "Understanding the basis of graph signal processing via an intuitive example-driven approach," *IEEE Signal Process. Mag.*, vol. 36, no. 6, pp. 133–145, Nov. 2019.
[14] G. Leus, A. G. Marques, J. M. Moura, A. Ortega, and D. I. Shuman, "Graph signal processing: History, development, impact, and outlook," *IEEE Signal Process. Mag.*, vol. 40, no. 4, pp. 49–60, Jun. 2023.
[15] A. Sandryhaila and J. M. Moura, "Discrete signal processing on graphs," *IEEE Trans. Signal Process.*, vol. 61, no. 7, pp. 1644–1656, Apr. 2013.
[16] F. Gama, E. Isufi, G. Leus, and A. Ribeiro, "Graphs, convolutions, and neural networks: From graph filters to graph neural networks," *IEEE Signal Process. Mag.*, vol. 37, no. 6, pp. 128–138, Nov. 2020.
[17] E. Isufi, F. Gama, D. I. Shuman, and S. Segarra, "Graph filters for signal processing and machine learning on graphs," *IEEE Trans. Signal Process.*, vol. 72, pp. 4745–4781, 2024.
[18] C. Ye, R. Shafipour, and G. Mateos, "Blind identification of invertible graph filters with sparse inputs," in *Proc. Eur. Signal Process. Conf.*, Sep. 2018, pp. 121–125.
[19] L. Wang and Y. Chi, "Blind deconvolution from multiple sparse inputs," *IEEE Signal Process. Lett.*, vol. 23, no. 10, pp. 1384–1388, Oct. 2016.
[20] C. Ye and G. Mateos, "Blind deconvolution on graphs: Exact and stable recovery," *Signal Process.*, vol. 230, 2025, Art. no. 109864.
[21] E. Ceci and S. Barbarossa, "Small perturbation analysis of network topologies," in *Proc. Int. Conf. Acoust., Speech, Signal Process*., 2018, pp. 4194–4198.
[22] E. Ceci and S. Barbarossa, "Graph signal processing in the presence of topology uncertainties," *IEEE Trans. Signal Process.*, vol. 68, pp. 1558–1573, 2020.
[23] F. Gama, J. Bruna, and A. Ribeiro, "Stability properties of graph neural networks," *IEEE Trans. Signal Process.*, vol. 68, pp. 5680–5695, 2020.
[24] E. Ceci, Y. Shen, G. B. Giannakis, and S. Barbarossa, "Graph-based learning under perturbations via total least-squares," *IEEE Trans. Signal Process.*, vol. 68, pp. 2870–2882, 2020.
[25] S. Rey, V. M. Tenorio, and A. G. Marques, "Robust graph filter identification and graph denoising from signal observations," *IEEE Trans. Signal Process.*, vol. 71, pp. 3651–3666, 2023.
[26] V. M. Tenorio, S. Rey, and A. G. Marques, "Blind deconvolution of sparse graph signals in the presence of perturbations," in *Proc. Int. Conf. Acoust., Speech, Signal Process*., 2024, pp. 9406–9410.
[27] S. Segarra, A. G. Marques, G. Mateos, and A. Ribeiro, "Network topology inference from spectral templates," *IEEE Trans. Signal Inf. Process. Netw.*, vol. 3, no. 3, pp. 467–483, Sep. 2017.
[28] L. Peng and R. Vidal, "Block coordinate descent on smooth manifolds: Convergence theory and twenty-one examples," in *Proc. Conf. Parsimony Learn.*, 2025, pp. 1–31.
[29] P. J. Huber, "Robust estimation of a location parameter," *Ann. Math. Statist.*, vol. 35, no. 1, pp. 73–101, 1964.
[30] P.-A. Absil, R. Mahony, and R. Sepulchre, *Optimization Algorithms on Matrix Manifolds*. Princeton, NJ, USA: Princeton Univ. Press, 2008.
[31] N. Boumal, *An Introduction to Optimization on Smooth Manifolds*. Cambridge, U.K.: Cambridge Univ. Press, 2023.
[32] A. G. Marques, S. Segarra, and G. Mateos, "Signal processing on directed graphs: The role of edge directionality when processing and learning from network data," *IEEE Signal Process. Mag.*, vol. 37, no. 6, pp. 99–116, Nov. 2020.
[33] C. Ye and G. Mateos, "Learning to identify sources of network diffusion," in *Proc. Eur. Signal Process. Conf*., Sep. 2022, pp. 727–731.
[34] A. A. Hagberg, D. A. Schult, and P. J. Swart, "Exploring network structure, dynamics, and function using networkx," in *Proc. 7th Python Sci. Conf.*, G. Varoquaux, T. Vaught, and J. Millman, Eds., Pasadena, CA USA, 2008, pp. 11–15.
[35] P. Hagmann et al., "Mapping the structural core of human cerebral cortex," *PLoS Biol.*, vol. 6, no. 7, 2008, Art. no. e159.

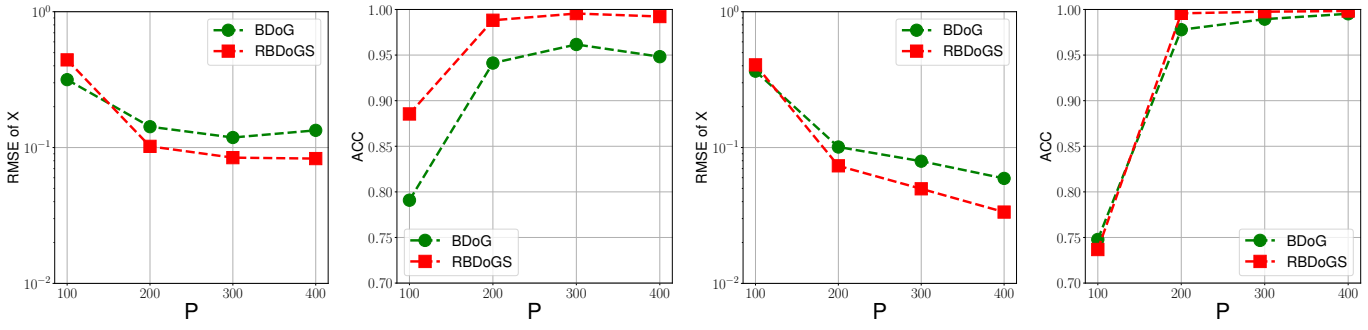

Fig. 4. Improved recovery performance of the RBDoGS algorithm on larger, real-world graphs: (a)- (b) Zachary's karate club in [34] with $N = 34$ nodes; (c) - (d) structural brain network studied in [35] with $N = 66$ nodes. (a) and (c) depict the RMSE of $\mathbf{X}$; while (b) and (d) show ACC_X for RBDoGS and the BDoG baseline that solves (3) with an imperfect $\mathbf{V}_p$ [18]. Median results over 20 independent realizations are consistent with those in Fig. 3.

SUPPLEMENTARY MATERIAL

Proof of Theorem 2

For GSO $\mathbf{S} = \mathbf{V}\mathbf{\Lambda}\mathbf{V}^\top$, we denote a polynomial graph filter with frequency response $\tilde{\mathbf{h}}$ as $\mathcal{P}(\tilde{\mathbf{h}}) := \mathbf{V}\text{diag}(\tilde{\mathbf{h}})\mathbf{V}^\top$. Besides, we consider the hollow matrix version of the graph filter $\mathcal{M}(\tilde{\mathbf{h}}) := (\mathbf{1}_N\mathbf{1}_N^\top - \mathbf{I}_N) \circ \mathcal{P}(\tilde{\mathbf{h}})$. We are given observations $\mathbf{Y} = \mathcal{P}(\tilde{\mathbf{h}}_0)\mathbf{X}_0$, where $\mathbf{X}_0 \in \mathbb{R}^{N\times P}$ is drawn from the Bernoulli-Gaussian model with sparsity level θ. Denote the support of $\mathbf{X}_0$ as $\mathcal{S} = \text{supp}(\mathbf{X}_0)$, and let $\mathbf{M}^{(\mathcal{S})}$ be the masked matrix with entries M_{ij} if $(i,j) \in \mathcal{S}$, and $M_{ij} = 0$ otherwise.

The observed, corrupted graph is $\mathbf{S}_p = \mathbf{V}_p\mathbf{\Lambda}_p\mathbf{V}_p^\top$ and we let $\mathbf{\Delta} := \mathbf{V} - \mathbf{V}_p$. Recall we wish to solve problem (3) and assume the exact recovery condition for the perfectly known GSO case ($\mathbf{\Delta} = \mathbf{0}_{N\times N}$) is satisfied, i.e., $\|\mathbf{P}_1^\perp\tilde{\mathbf{g}}_0\|_2 \leq a_0$, for some $a_0 \geq 0$ that does not depend on $\mathbf{\Delta}$ or $\tilde{\mathbf{g}}_0$. By applying the change of variables $\mathbf{w} = \tilde{\mathbf{g}} \circ \tilde{\mathbf{h}}_0$ and substituting it in $\mathbf{Y} = \mathcal{P}(\tilde{\mathbf{h}}_0)\mathbf{X}_0$, we have $\mathbf{V}_p\text{diag}(\tilde{\mathbf{g}})\mathbf{V}_p^\top\mathbf{Y} = \mathcal{P}(\mathbf{w})[\mathbf{X}_0 + \mathbf{E}]$, where $\mathbf{E} := (\mathbf{V} - \mathbf{\Delta})[\mathbf{\Delta}^\top - \text{diag}(\tilde{\mathbf{g}}_0)\mathbf{\Delta}^\top\mathcal{P}(\tilde{\mathbf{h}}_0)]\mathbf{X}_0$. Then, problem (3) can be equivalently rewritten as

$$\hat{\mathbf{w}} = \arg\min_{\mathbf{w}} \|\mathcal{P}(\mathbf{w})[\mathbf{X}_0 + \mathbf{E}]\|_{1,1}, \quad \text{s. to } \tilde{\mathbf{g}}_0^\top\mathbf{w} = N. \quad (13)$$

Note that if there is no eigenbasis perturbation, i.e., $\mathbf{V} = \mathbf{V}_p$, then $\hat{\mathbf{w}} = \mathbf{1}_N$ in (13) implies $\hat{\tilde{\mathbf{g}}}_p = \tilde{\mathbf{g}}_0$ in (3). In the presence of a perturbation $\mathbf{\Delta} \neq \mathbf{0}_{N\times N}$, $\hat{\tilde{\mathbf{g}}}_p - \tilde{\mathbf{g}}_0$ in (3) can be bounded in a similar way as $\hat{\mathbf{w}} - \mathbf{1}_N$ in (13), since $\hat{\tilde{\mathbf{g}}}_p - \tilde{\mathbf{g}}_0 = \tilde{\mathbf{g}}_0 \circ (\hat{\mathbf{w}} - \mathbf{1}_N)$. Also note that a feasible $\hat{\boldsymbol{\delta}} = \hat{\mathbf{w}} - \mathbf{1}_N$, e.g., $\tilde{\mathbf{g}}_0^\top\hat{\boldsymbol{\delta}} = 0$, can be decomposed as $\hat{\boldsymbol{\delta}} = -(\mathbf{a}^\top\hat{\mathbf{b}})\mathbf{1}_N + \hat{\mathbf{b}}$, where $\mathbf{a} = \mathbf{P}_1^\perp\tilde{\mathbf{g}}_0$ and $\hat{\mathbf{b}} = \mathbf{P}_1^\perp\hat{\boldsymbol{\delta}}$. Then, we have $\hat{\mathbf{w}} = [1 - (\mathbf{a}^\top\hat{\mathbf{b}})]\mathbf{1}_N + \hat{\mathbf{b}}$.

Our goal is to derive bounds for $\hat{\boldsymbol{\delta}}$. To this end, we have

$$\|\mathcal{P}(\hat{\mathbf{w}})[\mathbf{X}_0 + \mathbf{E}]\|_{1,1} \geq \|\mathcal{P}(\hat{\mathbf{w}})(\mathbf{X}_0 + \mathbf{E}^{(\mathcal{S})})\|_{1,1} - \|\mathcal{P}(\hat{\mathbf{w}})\mathbf{E}^{(\mathcal{S}^c)}\|_{1,1}. \quad (14)$$

As $\mathbf{E}^{(\mathcal{S})}$ has the same support as $\mathbf{X}_0$, it is sparse. From [20, Proposition 1], we lower bound the first summand in (14) as

$$\|\mathcal{P}(\hat{\mathbf{w}})(\mathbf{X}_0 + \mathbf{E}^{(\mathcal{S})})\|_{1,1} \geq \|\mathbf{X} + \mathbf{E}^{(\mathcal{S})}\|_{1,1} + PQ\|\hat{\mathbf{b}}\|_2, \quad (15)$$

where $Q := C_1\sqrt{\theta}\left(\sqrt{a_0^2 - (1-\sigma)^2\|\mathbf{a}\|_2^2} - \sigma\|\mathbf{a}\|_2\right)$, with some $\sigma := \frac{|\tilde{\mathbf{g}}_0^\top\mathbf{P}_1^\perp\hat{\mathbf{b}}|}{\|\hat{\mathbf{b}}\|\|\mathbf{P}_1^\perp\tilde{\mathbf{g}}_0\|} \in [0,1]$ and $C_1 > 0$. Note that we have assumed $\|\mathbf{a}\|_2 \leq a_0$, so $Q \geq 0$. Next, we upper bound $\|\mathcal{P}(\hat{\mathbf{w}})\mathbf{E}^{(\mathcal{S}^c)}\|_{1,1}$ in (14) as

$$\|\mathcal{P}(\hat{\mathbf{w}})\mathbf{E}^{(\mathcal{S}^c)}\|_{1,1} = \left\|\left(1 - \mathbf{a}^\top\hat{\mathbf{b}}\right)\mathbf{E}^{(\mathcal{S}^c)} + \mathcal{P}(\hat{\mathbf{b}})\mathbf{E}^{(\mathcal{S}^c)}\right\|_{1,1}$$
$$\leq \|\mathbf{E}^{(\mathcal{S}^c)}\|_{1,1} + (a_0\|\mathbf{E}^{(\mathcal{S}^c)}\|_{1,1} + \|[\mathbf{E}^{(\mathcal{S}^c)}]^\top\mathbf{V} \odot \mathbf{V}\|_{1\to 2})\|\hat{\mathbf{b}}\|_2. \quad (16)$$

Recall $\mathbf{1}_N$ should be the 'ideal' perturbation-free solution of (13), so $N = \tilde{\mathbf{g}}_0^\top\mathbf{1}_N$. For optimality, we must have

$$\|\mathcal{P}(\hat{\mathbf{w}})[\mathbf{X}_0 + \mathbf{E}]\|_{1,1} \leq \|\mathcal{P}(\mathbf{1}_N)[\mathbf{X}_0 + \mathbf{E}]\|_{1,1} = \|\mathbf{X} + \mathbf{E}^{(\mathcal{S})}\|_1 + \|\mathbf{E}^{(\mathcal{S}^c)}\|_{1,1}. \quad (17)$$

From (14)-(17), we find

$$\|\mathbf{X} + \mathbf{E}^{(\mathcal{S})}\|_{1,1} + \|\mathbf{E}^{(\mathcal{S}^c)}\|_{1,1} \geq \|\mathbf{X} + \mathbf{E}^{(\mathcal{S})}\|_{1,1} - \|\mathbf{E}^{(\mathcal{S}^c)}\|_{1,1} + (PQ - a_0\|\mathbf{E}^{(\mathcal{S}^c)}\|_{1,1} - \|[\mathbf{E}^{(\mathcal{S}^c)}]^\top\mathbf{V} \odot \mathbf{V}\|_{1\to 2})\|\hat{\mathbf{b}}\|_2$$

and if $PQ - a_0\|\mathbf{E}^{(\mathcal{S}^c)}\|_{1,1} - \|[\mathbf{E}^{(\mathcal{S}^c)}]^\top\mathbf{V} \odot \mathbf{V}\|_{1\to 2} > 0$, then

$$\|\hat{\mathbf{b}}\|_2 \leq \frac{2\|\mathbf{E}^{(\mathcal{S}^c)}\|_{1,1}}{PQ - a_0\|\mathbf{E}^{(\mathcal{S}^c)}\|_{1,1} - \|[\mathbf{E}^{(\mathcal{S}^c)}]^\top\mathbf{V} \odot \mathbf{V}\|_{1\to 2}}. \quad (18)$$

Because $\hat{\tilde{\mathbf{g}}} = \tilde{\mathbf{g}}_0 \circ \hat{\mathbf{w}}$, the difference vector between $\hat{\tilde{\mathbf{g}}}$ and the 'ideal' ground-truth $\tilde{\mathbf{g}}_0$ is $\mathbf{d}_g = \hat{\tilde{\mathbf{g}}} - \tilde{\mathbf{g}}_0 = \tilde{\mathbf{g}}_0 \circ \mathbf{w} - \tilde{\mathbf{g}}_0 = \tilde{\mathbf{g}}_0 \circ (\hat{\mathbf{w}} - \mathbf{1}_N) = \tilde{\mathbf{g}}_0 \circ \hat{\boldsymbol{\delta}}$. Recalling that $\hat{\boldsymbol{\delta}} = -\frac{\tilde{\mathbf{g}}_0^\top\hat{\mathbf{b}}}{N} + \hat{\mathbf{b}} = \left(\mathbf{I}_N - \mathbf{1}_N\frac{\tilde{\mathbf{g}}_0^\top}{N}\right)\hat{\mathbf{b}}$, we can bound the ℓ_2 norm of $\mathbf{d}_g$ as

$$\|\mathbf{d}_g\|_2 = \|\tilde{\mathbf{g}}_0 \circ \hat{\boldsymbol{\delta}}\|_2 = \left\|\text{diag}(\tilde{\mathbf{g}}_0)\left(\mathbf{I}_N - \mathbf{1}_N\frac{\tilde{\mathbf{g}}_0^\top}{N}\right)\hat{\mathbf{b}}\right\|_2$$
$$\leq \sigma_{\max}\left[\text{diag}(\tilde{\mathbf{g}}_0)\left(\mathbf{I}_N - \mathbf{1}_N\frac{\tilde{\mathbf{g}}_0^\top}{N}\right)\right]\|\hat{\mathbf{b}}\|_2,$$

which together with (18), completes the proof. ■

Numerical tests with larger, real-world graphs

To further assess recovery performance on larger real-world networks, we tested the RBDoGS algorithm on: (i) the 34-node Zachary's Karate Club graph [34]; and (ii) the 66-node structural brain network studied in [35]. We followed the same experimental protocol as in Test case 2. Fig. 4 shows the recovery performance in terms of RE_X and ACC_X, for RBDoGS and the BDoG baseline. Across graphs (i) and (ii), the results are consistent with the findings in Section V.